Molecular-dynamics force models for better control of energy dissipation in numerical simulations of dense granular media

L. Pournin* and Th. M. Liebling†
EPFL Swiss Federal Institute of Technology, CH-1015 Lausanne, Switzerland

A. Mocellin
Ecole des Mines de Nancy, Parc de Saurupt, 54042 Nancy cedex, France
(Received 10 May 2001; published 14 December 2001)

We first describe the three-dimensional extension of the molecular-dynamics models for granular media simulations. We then discuss the known energy dissipation problem occurring when simulating dense granular media with the usual molecular-dynamics forces models. We finally propose a force model able to control the energy dissipation in the multiparticle contact situations typical to dense granular media, together with appropriate numerical results.

DOI: 10.1103/PhysRevE.65.011302 PACS number(s): 45.70.−n, 83.10.Rs

I. INTRODUCTION

To perform computer simulations of granular media, one has to know how to handle the physical behavior of the contacts that may eventually take place between the grains. Two different approaches exist on that matter. The first one is to assume an expression for the repulsive force acting between the grains, which leads to molecular-dynamics models, and the second one is to instantaneously change the direction and value of the velocities according to conservation equations each time a contact occurs, this second approach leads to event-driven models. We will here focus on the molecular-dynamics models, and especially on what happens energetically with those models at a contact point for dense media, or in other words, for multiparticle contacts. Multiparticle contacts occur when a particle experiences contacts with several other particles at the same time so that those contacts have a direct influence on each other. Recalling that the molecular-dynamics models assume that contacts are independent from one another, we are dealing with a situation that is theoretically beyond the model capabilities. Unfortunately, it is common in practical simulations to experience multiparticle contacts, as simulations of dense media are widely performed. Several papers by Luding *et al.* [1] stress that if we do not know quantitatively how the energy is dissipated at a contact in a real granular medium, how much energy is dissipated in simulated media for multiparticle contacts is still a subject for discussions. As shown in [1], for multiparticle contacts, molecular-dynamics models may lead to a much too low energy dissipation, whereas event-driven models may lead to a much too high energy dissipation. In the latter case, the inelastic collapse phenomenon [2], in which the whole energy of the system is dissipated supports this conclusion. With the molecular-dynamics models, the lack of energy dissipation has also been noticed by Müller [3], who performed simulations of a rock falling on a granular bed, which came in agreement with real experiments when an external friction coefficient between air and grains was artificially added. We will investigate here this kind of energy dissipation obtained with molecular-dynamics models for multiparticle contacts and bring different ideas on how to improve it.

II. MOLECULAR-DYNAMICS MODELS

We introduce here the molecular-dynamics models with spherical particles. This shape makes the explanations easier and does not cause the model to be in any way less meaningful. Attempts to adapt molecular-dynamics models to nonspherical particles have been made and the reader may refer to [4] for more information on this subject. Let G_1 and G_2 be two spherical grains in a three-dimensional space (both with their characteristic radius R_i, mass m_i, inertia moment I_i, position $\boldsymbol{x}_i$ of the mass center, linear speed $\boldsymbol{v}_i$, and spin vector $\boldsymbol{\omega}_i$, for $i \in \{1,2\}$) experiencing a contact with each other at point C. Let $\mathcal{P}$ be the plane tangent to G_1 and G_2 at point C. We can define a unitary vector $\boldsymbol{u}_n$ normal to $\mathcal{P}$ as

$$\boldsymbol{u}_n = \frac{\boldsymbol{x}_2 - \boldsymbol{x}_1}{\|\boldsymbol{x}_2 - \boldsymbol{x}_1\|}, \tag{1}$$

and the relative velocity $\boldsymbol{v}_c$ of G_1 and G_2 at point C

$$\boldsymbol{v}_c = \dot{\boldsymbol{x}}_2 - \dot{\boldsymbol{x}}_1 + \boldsymbol{u}_n \wedge (R_1\boldsymbol{\omega}_1 + R_2\boldsymbol{\omega}_2). \tag{2}$$

In the molecular-dynamics models, grains overlap whenever a contact occurs, which allows us to quantify the deformation the grains experience at the contact point thanks to the vector quantity $\boldsymbol{\xi}$, whose projection ξ_n on $\boldsymbol{u}_n$ is shown in Fig. 1. Consider the differential equation

$$\dot{\boldsymbol{\xi}} = (\boldsymbol{u}_n \wedge \dot{\boldsymbol{u}}_n) \wedge \boldsymbol{\xi} - \boldsymbol{v}_c. \tag{3}$$

We define the overlap $\boldsymbol{\xi}$ as the solution of Eq. (3) for which $\boldsymbol{\xi} = \boldsymbol{0}$ when the contact begins. The normal and tangential overlaps ξ_n and $\boldsymbol{\xi}_t$ are then given by

*Electronic address: lionel.pournin@gmx.fr
†Electronic address: thomas.liebling@epfl.ch

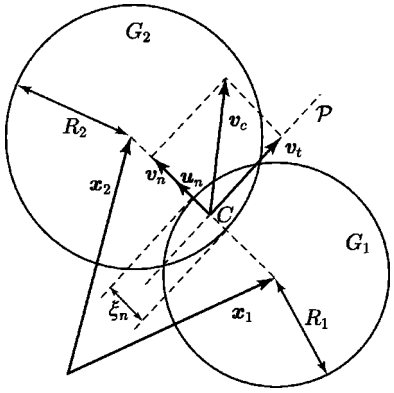

FIG. 1. A contact between two grains G_1 and G_2 with the molecular-dynamics models.

$$\xi_n = \boldsymbol{\xi}\cdot\boldsymbol{u}_n\,,$$
$$\boldsymbol{\xi}_t = \boldsymbol{\xi} - (\boldsymbol{\xi}\cdot\boldsymbol{u}_n)\boldsymbol{u}_n\,. \tag{4}$$

From Eqs. (1), (2), and (4), the time derivative of the normal overlap reads

$$\dot{\xi}_n = -\boldsymbol{v}_c\cdot\boldsymbol{u}_n\,. \tag{5}$$

Note that with Eq. (2), Eq. (5) simplifies to what intuition suggests: $\xi_n = R_1 + R_2 - \|\boldsymbol{x}_2 - \boldsymbol{x}_1\|$. Let $\boldsymbol{u}_t$ be a unit vector normal to $\boldsymbol{u}_n$, which follows the motion of plane $\mathcal{P}$, which is such that $\dot{\boldsymbol{u}}_t = (\boldsymbol{u}_n \wedge \dot{\boldsymbol{u}}_n)\wedge\boldsymbol{u}_t$. If $\xi_t = \boldsymbol{\xi}_t\cdot\boldsymbol{u}_t$, then

$$\dot{\xi}_t = -\boldsymbol{v}_c\cdot\boldsymbol{u}_t\,. \tag{6}$$

Let $\boldsymbol{f}_{G_1\to G_2}$ and $\boldsymbol{f}_{G_2\to G_1}$ be the forces applied, respectively, to G_2 and G_1 at the contact point. Equilibrium conditions give $\boldsymbol{f}_{G_1\to G_2} = -\boldsymbol{f}_{G_2\to G_1}$. Therefore, in the following, we will use exclusively the quantity $\boldsymbol{f}_{G_1\to G_2}$, which we will simply denote $\boldsymbol{f}$. In the molecular-dynamics procedure, the contact forces are computed as functions of the overlaps ξ_n and $\boldsymbol{\xi}_t$ and their time derivatives $\dot{\xi}_n$ and $\dot{\boldsymbol{\xi}}_t$,

$$\boldsymbol{f} = \phi_n(\xi_n,\dot{\xi}_n)\boldsymbol{u}_n + \boldsymbol{\phi}_t(\boldsymbol{\xi}_t,\dot{\boldsymbol{\xi}}_t), \tag{7}$$

where $\boldsymbol{\phi}_t$ is a vector quantity parallel to the contact plane $\mathcal{P}$. Assuming that the tangential force $\boldsymbol{\phi}_t(\boldsymbol{\xi}_t,\dot{\boldsymbol{\xi}}_t)$ does not already take into account the Coulomb friction, one has to replace it in Eq. (7) by

$$\boldsymbol{\phi}_t^C(\boldsymbol{\xi}_t,\dot{\boldsymbol{\xi}}_t) = \min[\mu\phi_n(\xi_n,\dot{\xi}_n), \|\boldsymbol{\phi}_t(\boldsymbol{\xi}_t,\dot{\boldsymbol{\xi}}_t)\|]\boldsymbol{u}_t\,, \tag{8}$$

where μ is the friction coefficient, and

$$\boldsymbol{u}_t = \begin{cases} \dfrac{\boldsymbol{\phi}_t(\boldsymbol{\xi}_t,\dot{\boldsymbol{\xi}}_t)}{\|\boldsymbol{\phi}_t(\boldsymbol{\xi}_t,\dot{\boldsymbol{\xi}}_t)\|} & \text{if } \boldsymbol{\phi}_t(\boldsymbol{\xi}_t,\dot{\boldsymbol{\xi}}_t)\neq\boldsymbol{0}, \\ \boldsymbol{0} & \text{if } \boldsymbol{\phi}_t(\boldsymbol{\xi}_t,\dot{\boldsymbol{\xi}}_t)=\boldsymbol{0}. \end{cases} \tag{9}$$

Here are two examples of force models, which are the most frequently used ones for practical simulations. We describe those models without the Coulomb friction, which has to be added afterwards according to Eq. (8).

Viscoelastic force. This force, proposed by Cundall and Strack [5] is a linear combination of elastic and viscous terms. Energy is dissipated at the contact point by the viscous term. We give the linear expression of this force, but nonlinear versions have been proposed and investigated (see [6])

$$\phi_n(\xi_n,\dot{\xi}_n) = k_n\xi_n + c_n\dot{\xi}_n\,, \tag{10}$$

$$\boldsymbol{\phi}_t(\boldsymbol{\xi}_t,\dot{\boldsymbol{\xi}}_t) = k_t\boldsymbol{\xi}_t + c_t\dot{\boldsymbol{\xi}}_t\,. \tag{11}$$

Walton force. This force, which models the elastoplastic behavior of the grains at the contact point was proposed by Walton and Braun [7]. The energy is dissipated at a contact as plastic deformation. The loading is assumed elastoplastic and the unloading elastic. In either loading and unloading phases, the force is taken as a linear function of the overlap. As the force only depends on the overlap, the loading-unloading paths obtained with the Walton force model may be drawn on a force-overlap diagram, as sketched on Fig. 2, left. In order to take into account the elastoplastic loading, the loading slope $k^{(1)}$ has to be lower than the purely elastic unloading slope $k^{(2a)}$. If a reloading takes place, the force follows a purely elastic slope until it reaches the first loading path [this corresponds to part (3) on the left diagram of Fig. 2]. It would have been more realistic to model the loading phase as a first purely elastic part followed by a plastic part, and to take into account the 3/2 exponent given by the Hertz theory for the elastic part, but this simple model contains the overall behavior of elastoplastic materials and is therefore sufficient for a first approximation. The normal force reads

$$\phi_n(\xi_n,\dot{\xi}_n) = \begin{cases} \min[\phi_n^{(2a)}, k_n^{(1)}\xi_n] & \text{for } \dot{\xi}_n > 0, \\ \max[\phi_n^{(2a)}, 0] & \text{for } \dot{\xi}_n < 0. \end{cases} \tag{12}$$

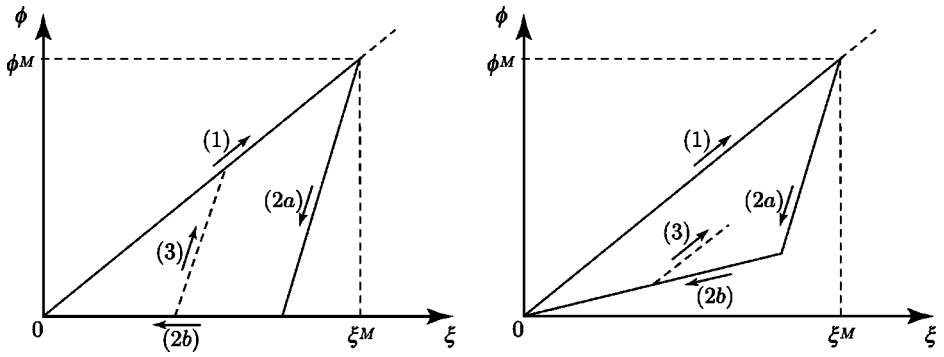

FIG. 2. Behavior of force-overlap paths for Walton force model (left) and the other model (right). For each model the diagram may be used either for a normal or a tangential force. The paths divide in (1): loading, $(2a,2b)$: unloading, (3): reloading.

In Eq. (12),

$$\phi_n^{(2a)} = k_n^{(2a)}(\xi_n - \xi_n^M) + \phi_n^M, \tag{13}$$

where ξ_n^M and ϕ_n^M are the values of ξ_n and ϕ_n at the instant $\dot{\xi}_n$ last changed signs, either from positive to negative or from negative to positive (see Fig. 2, left diagram). A simple expression for the tangential Walton force roughly takes the same features as the normal Walton force,

$$\boldsymbol{\phi}_t(\boldsymbol{\xi}_t, \dot{\boldsymbol{\xi}}_t) = \begin{cases} \min[\phi_t^{(2a)}, k_t^{(1)}\xi_t]\boldsymbol{u}_t & \text{for } \dot{\xi}_t > 0, \\ \max[\phi_t^{(2a)}, 0]\boldsymbol{u}_t & \text{for } \dot{\xi}_t < 0. \end{cases} \tag{14}$$

In Eq. (14),

$$\phi_t^{(2a)} = k_t^{(2a)}(\xi_t - \xi_t^M) + \phi_t^M, \tag{15}$$

where ξ_t^M and ϕ_t^M are the values of ξ_t and ϕ_t at the instant $\dot{\xi}_t$ last changed signs, either from positive to negative or from negative to positive and $\boldsymbol{u}_t$ is the unit vector defined when $\boldsymbol{\xi}_t \neq \boldsymbol{0}$ by $\boldsymbol{u}_t = \boldsymbol{\xi}_t / \xi_t$. Both ϕ_n and $\|\boldsymbol{\phi}_t\|$ may be drawn as functions of the overlaps (respectively, ξ_n or ξ_t) on a force-overlap diagram as the left one of Fig. 2.

Those two force models are the most used in simulations, and we will focus on them in the following as other models that have been developed (see, for example, [6,8]) usually are improvements of those two.

III. TUNING MOLECULAR-DYNAMICS MODELS WITH REAL EXPERIMENTS

The molecular-dynamics models described in Sec. II are technically operational, but the parameters of the force models (k_n, k_t, c_n, c_t for the viscoelastic model and $k_n^{(1)}$, $k_t^{(1)}$, $k_n^{(2a)}$, $k_t^{(2a)}$ for the Walton model) do not have a true physical reality, which means they have no *a priori* expressions for which the modeled behavior will be realistic. Those parameters then have to be set empirically, so that the model quantitatively reproduces some real and well-known experiments. Experiments that involve more than one contact at a time usually do not provide measures that allow any analytic linking between the experiment and the model parameters, the number of cases to investigate for the resolution would be too high, and numerical implementation would be very heavy. We are left with single contact experiments to set our parameters, with no guarantee that situations that involve several simultaneous contacts will then be realistically modeled.

The experiment we will work with is the collision of two grains G_1 and G_2 having no initial spin. Three key quantities can be measured: the duration of the contact t_c and the normal and tangential restitution coefficients e_n and e_t, defined as follows using the notations of Sec. II:

$$e_n = -\frac{\dot{\xi}_n^f}{\dot{\xi}_n^i}, \qquad e_t = -\frac{\dot{\xi}_t^f}{\dot{\xi}_t^i}, \tag{16}$$

where i and f as exponents refer to quantities immediately before and immediately after the collision. Note that e_t depends on the impact angle when the contact is slippery but is constant for a sticky contact. In this section, we assume the contact is and remains sticky. The tangential restitution coefficient then has a fixed value. This also allows us to use directly Eq. (7), without Coulomb friction for the analytic resolutions. The slippery behavior of the contact, together with the subsequent alteration of e_t will be provided afterwards through Eq. (8). We will find here the analytic expressions for t_c, e_n, and e_t for the modeled contact as functions of the model parameters. By inverting those expressions, we will be able to set the model parameters so that e_n, e_t, and t_c are controlled for single contact situations. The motion equations for the grains G_1 and G_2 read

$$\begin{aligned} m_1\ddot{\boldsymbol{x}}_1 &= -\boldsymbol{f}, \\ m_2\ddot{\boldsymbol{x}}_2 &= \boldsymbol{f}, \\ I_1\dot{\boldsymbol{\omega}}_1 &= -R_1\boldsymbol{u}_n \wedge \boldsymbol{f}, \\ I_2\dot{\boldsymbol{\omega}}_2 &= -R_2\boldsymbol{u}_n \wedge \boldsymbol{f}. \end{aligned} \tag{17}$$

As the two grains experience the collision, plane $\mathcal{P}$ will not move much, which allows us to assume $\boldsymbol{u}_n$ is a constant. Equation (3) then simplifies to $\dot{\boldsymbol{\xi}} = -\boldsymbol{v}_c$ and Eq. (2) gives

$$\ddot{\boldsymbol{\xi}} = \ddot{\boldsymbol{x}}_1 - \ddot{\boldsymbol{x}}_2 - \boldsymbol{u}_n \wedge (R_1\dot{\boldsymbol{\omega}}_1 + R_2\dot{\boldsymbol{\omega}}_2). \tag{18}$$

From Eqs. (17) and (18), one finds

$$\ddot{\boldsymbol{\xi}} = -\frac{1}{m_{eff}}\boldsymbol{f} - \left(\frac{R_1^2}{I_1} + \frac{R_2^2}{I_2}\right)\boldsymbol{\phi}_t(\boldsymbol{\xi}_t, \dot{\boldsymbol{\xi}}_t), \tag{19}$$

where $1/m_{eff} = 1/m_1 + 1/m_2$. As the grains have no initial spin, the centers of the grains will move in a plane. Calling $\boldsymbol{u}_\perp$ a unit vector normal to that plane, we define a unit vector tangential to the contact by $\boldsymbol{u}_t = \boldsymbol{u}_n \wedge \boldsymbol{u}_\perp$. Equation (19) then projects on $\boldsymbol{u}_n$ and $\boldsymbol{u}_t$ as follows:

$$\begin{aligned} \ddot{\xi}_n &= -\frac{1}{m_{eff}}\phi_n(\xi_n, \dot{\xi}_n), \\ \ddot{\xi}_t &= -\left(\frac{1}{m_{eff}} + \frac{R_1^2}{I_1} + \frac{R_2^2}{I_2}\right)\boldsymbol{\phi}_t(\boldsymbol{\xi}_t, \dot{\boldsymbol{\xi}}_t) \cdot \boldsymbol{u}_t. \end{aligned} \tag{20}$$

Where $\xi_t = \boldsymbol{\xi}_t \cdot \boldsymbol{u}_t$. Those differential equations may be solved for ξ_n and ξ_t, based upon expressions for ϕ_n and $\boldsymbol{\phi}_t$ such as Eqs. (10) and (11) or Eqs. (12) and (14). For those two cases, we have the following solutions:

Viscoelastic force. From Eqs. (10), (11), and (20) we find the following set of differential equations:

$$\ddot{\xi}_n+\frac{c_n}{m_{eff}}\dot{\xi}_n+\frac{k_n}{m_{eff}}\xi_n=0,$$
$$\ddot{\xi}_t+c_t\left(\frac{1}{m_{eff}}+\frac{R_1^2}{I_1}+\frac{R_2^2}{I_2}\right)\dot{\xi}_t+k_t\left(\frac{1}{m_{eff}}+\frac{R_1^2}{I_1}+\frac{R_2^2}{I_2}\right)\xi_t=0. \tag{21}$$

Solving Eq. (21) provides expressions for e_n, e_t, and t_c according to Eq. (16) as functions of k_n, c_n, k_t, and c_t. Inverting those expressions, we find

$$k_n=\frac{m_{eff}}{t_c^2}[\pi^2+\ln(e_n)^2],$$
$$c_n=-\frac{2m_{eff}}{t_c}\ln(e_n),$$
$$k_t=\frac{1}{t_c^2\left(\frac{1}{m_{eff}}+\frac{R_1^2}{I_1}+\frac{R_2^2}{I_2}\right)}[\pi^2+\ln(e_t)^2],$$
$$c_t=-\frac{1}{t_c\left(\frac{1}{m_{eff}}+\frac{R_1^2}{I_1}+\frac{R_2^2}{I_2}\right)}\ln(e_t). \tag{22}$$

The set of equations (22) allows us to control the values of e_n, e_t, and t_c for single sticky contacts situations with the viscoelastic force model.

Walton force. From Eqs. (12), (14), and (20) we find the following differential equations:

$$\ddot{\xi}_n+\frac{k_n^{(1)}}{m_{eff}}\xi_n=0 \quad \text{for} \quad \dot{\xi}_n>0,$$
$$\ddot{\xi}_t+k_t^{(1)}\left(\frac{1}{m_{eff}}+\frac{R_1^2}{I_1}+\frac{R_2^2}{I_2}\right)\xi_t=0 \quad \text{for} \quad \dot{\xi}_t>0,$$
$$\ddot{\xi}_n+\frac{k_n^{(2a)}}{m_{eff}}\xi_n-\frac{k_n^{(2a)}-k_n^{(1)}}{m_{eff}}\xi_n^M=0 \quad \text{for} \quad \dot{\xi}_n<0,$$
$$\ddot{\xi}_t+\left(\frac{1}{m_{eff}}+\frac{R_1^2}{I_1}+\frac{R_2^2}{I_2}\right)\times[k_t^{(2a)}\xi_t-(k_t^{(2a)}-k_t^{(1)})\xi_t^M]=0 \quad \text{for} \quad \dot{\xi}_t<0, \tag{23}$$

where the quantities ξ_n^M and ξ_t^M refer to the values of ξ_n and ξ_t at the end of the loading phases. Solving Eq. (23) for solutions with continuous derivatives gives expressions for e_n, e_t, and t_c according to Eq. (16) as functions of k_n, c_n, k_t, and c_t. Inverting those expressions, we find

$$k_n^{(1)}=m_{eff}\left(\frac{\pi(1+e_n)}{2t_c}\right)^2,$$
$$k_n^{(2a)}=m_{eff}\left(\frac{\pi(1+e_n)}{2t_ce_n}\right)^2,$$
$$k_t^{(1)}=\frac{1}{\frac{1}{m_{eff}}+\frac{R_1^2}{I_1}+\frac{R_2^2}{I_2}}\left(\frac{\pi(1+e_t)}{2t_c}\right)^2,$$
$$k_t^{(2a)}=\frac{1}{\frac{1}{m_{eff}}+\frac{R_1^2}{I_1}+\frac{R_2^2}{I_2}}\left(\frac{\pi(1+e_t)}{2t_ce_t}\right)^2. \tag{24}$$

Equations (24) allow us to control the values of e_n, e_t, and t_c for single sticky contacts situations with the Walton force model.

By expressing the coefficients of the force models as shown in this section, we know that any single sticking contact situation will be realistically modeled. However, we have no guarantee that situations involving several simultaneous contacts will be realistic.

IV. ENERGY DISSIPATION FOR MULTIPARTICLE CONTACTS WITH THE MOLECULAR-DYNAMICS MODELS

In Sec. III, we found expressions for the parameters ruling the behavior of the force model such that single contact experiments are realistically modeled. With those expressions, however, we do not have any guarantee that multiparticle contacts will be accurate. We investigate here the behavior of normal forces for multiparticle contacts when using expressions found in Sec. III for the model parameters, pointing out that energy dissipation is then too low for quasistatic multiparticle contacts.

A. Experimental setup

We use a set of n identical beads vertically stacked over a bottom plate as shown in [1]. The initial distance between neighboring beads and between the bottom bead and the bottom plate is strictly positive, equal to l_i. Gravity is set to 0, energy being brought to the system through the initial velocity $v_i<0$, common to each of the beads. The beads are constrained to move vertically. Contacts are indexed from 1 for the contact between the bottom plate and the bead at the bottom of the stack to n for the contact between the two topmost beads. This setup is represented on Fig. 3, with useful notations.

When performing this simulation, the beads fall and contacts occur in the stack. For small values of l_i, contact intervals overlap; multiparticle contacts then take place. The stack will eventually reach a state where all the beads move upwards with velocities decreasing from the top of the stack, ensuring that no further contact will take place. We may then measure the ratio ϵ of the final total kinetic energy over the initial total kinetic energy. This ratio measures the energy loss due to the contacts that took place inside the stack. We

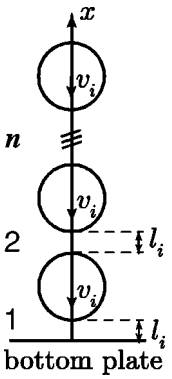

FIG. 3. Experimental setup. Contacts numbered starting at plate.

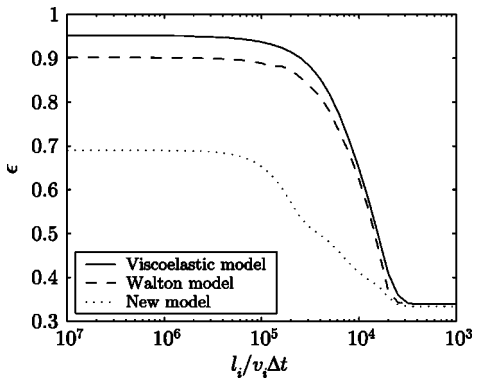

FIG. 4. Energy dissipated for multiparticle contacts with some molecular-dynamics force models.

also measure the force-overlap path for each contact. The energy dissipated at a contact is the surface in the force-overlap plane that is delimited by the force-overlap path.

B. Energy dissipation with the usual force models

As written in [1], ϵ only depends on the value of $l_i/v_i\Delta t$, independently of the values of v_i, Δt and l_i taken separately. Plotting ϵ against $l_i/v_i\Delta t$ leads to the curves shown on Fig. 4. Reference [1] concludes that for dense granular media (small values of l_i), no matter how small the value of Δt, the dissipated energy will be about ten percent of the initial energy, which may be too low, in particular, this leads in [3] to very unrealistic behaviors. We compare the energy dissipated at each contact when $l_i=0$ m and $l_i=5\times10^{-4}$ m on Fig. 8 with the viscoelastic and Walton force models. When $l_i=5\times10^{-4}$ m, all the contacts that occur are single contacts and the energy dissipation is therefore accurate for the two force models discussed here. When $l_i=0$, multiparticle contacts take place and we see that the energy dissipated at each contact is very much lower than for the previous case. In Fig. 5, we show the force-overlap paths obtained with $v_i=-0.2$ m/s, $l_i=0$, for contacts 1 (between the bottom plate and the bead lying on it), 4, 7, and 10 (between the two topmost beads) either for the viscoelastic and the Walton force models. Note that the slope for the first loading of the first contact is twice that of the other contacts, this is because this contact is between a bead and the bottom plate where mass is infinite. We see that either for the viscoelastic or the Walton force models, there is plenty of space available in the force-overlap diagram to dissipate energy. This space is not used by any of those models and the additional dissipation brought by the multiparticle contacts is restricted to a small hysteretic surface (circled by a spiral for the viscoelastic model and by triangles for the Walton model). One idea would be to use more of the space available in the force-overlap diagram.

V. USING AVAILABLE SPACE IN THE FORCE-OVERLAP DIAGRAM

The Walton force model gives an expression of the force that only depends on the overlap. It is then easy to represent the force-overlap path. This kind of path for the Walton model is shown on the left diagram of Fig. 2. A cycle of loading-unloading may take place in the part $(2a)$, leading to no energy dissipation at all. Instead of taking a purely elastic slope for reloadings, we may assume reloadings are elasto-plastic, with the same properties as the first loading. This modifies the part (3) on the left diagram of Fig. 2 to that on the right diagram, as any reloading phase then has the slope $k^{(1)}$. Unfortunately, the overlap may then grow indefinitely with a bounded force, which leads to the model dissipating all available energy. That is why we impose the last part $(2b)$ of the unloading path to be elastic with a strictly positive fixed slope, as shown on the right diagram of Fig. 2. Otherwise stated, we use here (ϕ,ξ) either for (ϕ_n,ξ_n) or $(\|\boldsymbol{\phi}_t\|,\xi_t)$, thus describing the normal and tangential force models at the same time. We will now quantify exactly how much energy will be lost with this model every time a contact occurs. In order to do that, we introduce the energy E stored in a contact as

$$\dot{E}=\phi(t)\dot{\xi}, \tag{25}$$

with $E=0$ when the contact begins. The energy dissipated by the contact is the surface circled by the path of the force on a force-overlap diagram. Assuming an unloading phase begins at point (ξ,ϕ) on such a diagram, with some energy E stored in the contact we may express $k^{(2a)}$ so that the part of E dissipated in this unloading phase is $(1-e_n^2)E$ if no reloading takes place

$$k^{(2a)}=\frac{\phi-k^{(2b)}\xi_\cap}{\xi-\xi_\cap}, \tag{26}$$

where $\xi_\cap$ is the value of ξ for which $(2a)$ and $(2b)$ intersect,

$$\xi_\cap=\frac{\phi\xi-2e_n^2E}{\phi-k^{(2b)}\xi}. \tag{27}$$

With Eqs. (26) and (27) the energy dissipated at the end of the contact will be $1-e_n^2$ times the total energy brought to the contact, no matter how many reloadings take place or when they take place. Equations (26) and (27) express the slope $k^{(2a)}$ as a function of $k^{(2b)}$ and of (ξ,ϕ,E), which is the state of the contact at the begining of the unloading. We

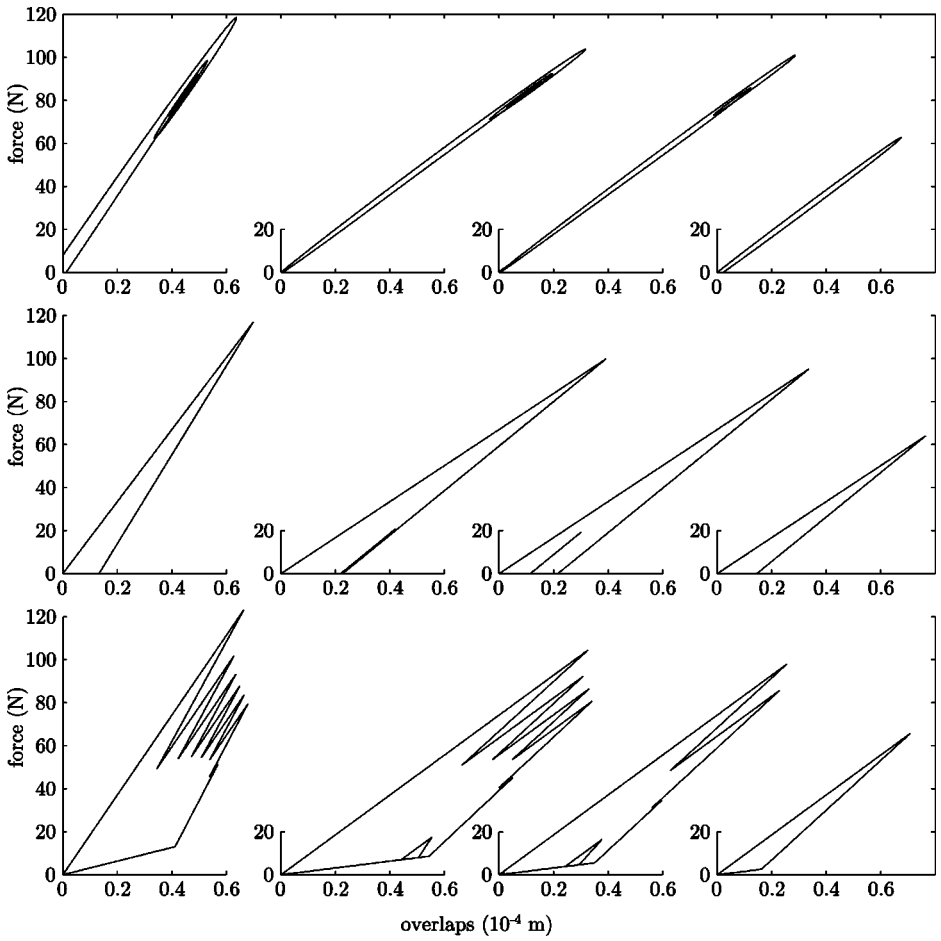

FIG. 5. Force-overlap paths for the viscoelastic model (top), the Walton model (middle), and the other model (bottom). Those paths are drawn for contacts 1, 4, 7, and 10 from left to right.

still have to set values for $k^{(1)}$ and $k^{(2b)}$. $k^{(1)}$ controls the duration of the loading phase for a single contact. Solving the motion equations for a single contact, one finds the following expressions for $k^{(1)}$ for either normal or tangential forces:

$$k_n^{(1)} = m_{eff}\left(\frac{\pi}{2t^{(1)}}\right)^2,$$
$$k_t^{(1)} = \frac{1}{\frac{1}{m_{eff}} + \frac{R_1^2}{I_1} + \frac{R_2^2}{I_2}}\left(\frac{\pi}{2t^{(1)}}\right)^2, \tag{28}$$

where $t^{(1)}$ is the duration of the loading phase for a single contact. For the simulations, we take $t^{(1)} = (1/2)t_c$; that is, $t^{(1)}$ is half the duration of a single contact. We now discuss the value of the slope $k^{(2b)}$. Let α be

$$\alpha = \frac{k^{(2b)}}{k^{(1)}}. \tag{29}$$

Intuitively, when α nears 1, there is not enough space between (1) and $(2b)$ to dissipate energy, there is therefore a value above which α must not go. Integrating the force-overlap path for a single contact, one finds the inequality $\alpha \leqslant 1 - e_n^2$. As $k^{(2b)}$ is strictly positive, so is α and we have

$$0 < \alpha \leqslant 1 - e_n^2. \tag{30}$$

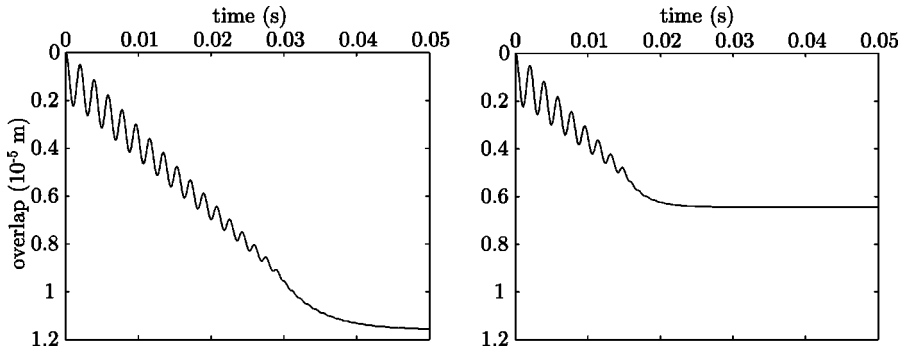

FIG. 6. Overlaps drawn against time for a bead subject to gravity lying on a plane and simulated with the model. On the left, $\alpha = 0.5$ and on the right $\alpha = 0.9$. In both cases, the bead weighs 0.188 kg.

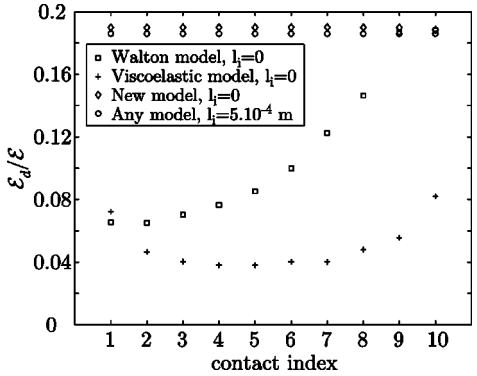

FIG. 7. Ratio of the energy dissipated at a contact over the total energy brought to this contact for all the contacts of the numerical experiment of Sec. IV. Contact index is 1 for the contact between the bottom plate and the stack of beads and 10 between the two topmost beads.

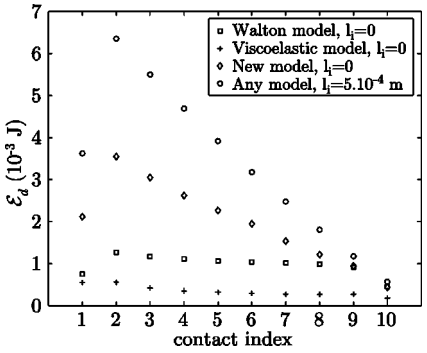

FIG. 8. Energy dissipated at each contact for various force models and for two values of l_i.

Now, consider a single bead subject to gravity lying on an horizontal plane. If the bead is initially tangent to the plane, it will slightly move down until an equlilibrium is reached after a time t_e with the force between the bead and the plane equal to the weight of the bead. The time t_e depends on the value of α. The larger α is, the smaller t_e will be, with a minimal value for t_e when α reaches its maximal value of $1-e_n^2$. In Fig. 6, the overlap is drawn against time for two values of α for this experiment of a bead lying on a plane. This figure shows that the stability is quicker for high values of α. Note that if $\alpha=0$, which violates Eq. (30), $t_e=+\infty$ as the overlap will grow infinite. In this case, potential energy transforms into kinetic energy and dissipates at the contact point, leading to the dissipation of an infinite amount of potential energy together with the bead moving downwards in the plane.

VI. ENERGY DISSIPATION WITH THE FORCE MODEL

We perform the experiment described in Sec. IV with the model, and compare the results with those obtained with Walton and viscoelastic models. Figure 4 shows that the total energy dissipated by the stack of beads is significantly higher for this model than for the previous ones, for small values of $l_i/v_i\Delta t$. Let $\mathcal{E}$ be the total energy brought to a contact, that is the work of the contact force in all loading and reloading phases, and $\mathcal{E}_d$ the amount of energy dissipated in the same contact. With Eqs. (26) and (27), the ratio $\mathcal{E}_d/\mathcal{E}$ is always equal to $(1-e_n^2)$, independently of the loading-unloading history of the contact. This was not the case for the force models of Sec. II. Performing the numerical experiment of Sec. IV, we draw on Fig. 7 the ratio $\mathcal{E}_d/\mathcal{E}$ for each contact and for all three force models. It is clear that the only model that controls the ratio $\mathcal{E}_d/\mathcal{E}$ is the one we propose in this section. Figure 7 shows that the case where all contacts are single ($l_i=5.10^{-4}$ m) is very similar to the multiparticle case ($l_i=0$ m) simulated with the model. Figure 8 shows that the energy dissipated at each contact is higher for this model than for the previous ones. We draw in Fig. 5 the force paths for contacts 1, 4, 7, and 10 with the force model. We see that the surface circled by the path is there greater than for the viscoelastic or the Walton force models.

VII. CONCLUSION

We described a molecular-dynamics model able to increase the energy dissipation in multiparticle contacts situations. With this model, it is possible to choose the fraction of the energy brought to the contact that will be dissipated, independently of the loading-unloading history of the contact, which is not the case for the usual force models. This feature, in comparison to the Walton force model is that loading-unloading cycles will take advantage of the room available in the force-overlap plane to dissipate more energy. However, some of the parameters of this model may still be improved, as for example, the slope of the loading/reloading phase that was taken equal to the slope of the loading phase of the Walton model (24). This slope could, for example, be changed from one reloading to the next one. Those parameters have to be validated with comparison to some additional experiments for further improvements of the model.

ACKNOWLEDGMENTS

This project was supported by DONET and by the Swiss National Science Foundation. We would like to thank J.-A. Ferrez for his constant help and L. Guy Raguin for the many fruitful discussions we had and for his clever comments on the last versions of this paper.

[1] S. Luding, E. Clément, A. Blumen, J. Rajchenbach, and J. Duran, Phys. Rev. E **50**, 4113 (1994).
[2] S. McNamara and W.R. Young, Phys. Fluids A **4**, 496 (1992).
[3] D. Müller, thèse no. 1545, EPFL (1996).
[4] H.-G. Matuttis, S. Luding, and H.J. Herrmann, Powder Technol. **109**, 278 (2000).
[5] P.A. Cundall and O.D.L. Strack, Geotechnique **29**, 47 (1979).
[6] G. Kuwabara and K. Kono, Jpn. J. Appl. Phys., Part 1 **26**, 1230 (1987).
[7] O.R. Walton and R.L. Braun, J. Rheol. **30**, 949 (1986).
[8] M.H. Sadd, Q. Tai, and A. Shukla, Int. J. Non-Linear Mech. **28**, 251 (1993).